

# Comparative Analysis on Mechanical Performance of Concrete Inclined Tension Rods with Square and Circular Steel Pipes in Cable-Stay Girder Anchorage Zone of Low-Pylon Cable-Stayed Bridge

Liang Zhang

Central South University of Forestry and Technology, Changsha, China

**How to cite this paper:** Zhang, L. (2026). Comparative analysis on mechanical performance of concrete inclined tension rods with square and circular steel pipes in cable-stay girder anchorage zone of low-ylon cable-stayed bridge. *Advances in Engineering Research: Possibilities and Challenges*, 4(2), 52–63. ISSN Print: 3079-5192; ISSN Online: 3079-5206. <https://doi.org/10.63313/AERpc.9103>  
**Published: 2026-05-11**

Copyright © 2026 by author(s) and Erytis Publishing Limited.  
This work is licensed under the Creative Commons Attribution International License (CC BY 4.0).  
<http://creativecommons.org/licenses/by/4.0/>



## Abstract

Aiming at the inherent performance bottlenecks of reinforced concrete (RC) inclined tension rods in the cable-girder anchorage zone of low-ylon cable-stayed bridges, such as low ductility and significant post-peak damage localization, an optimized scheme of prestressed concrete-filled steel tube (CFST) inclined tension rod is proposed. Taking the Luzhou Tuojiang Railway Super Large Bridge, a low-ylon cable-stayed bridge with a span arrangement of (146+292+146) m, as the engineering background, a three-dimensional nonlinear finite element model is established based on ANSYS APDL. The whole-process mechanical behaviors of three schemes, namely RC, square CFST and circular CFST inclined tension rods, under the most unfavorable cable force are comparatively analyzed, and the influence law of section form on mechanical performance is revealed from the perspective of confinement mechanism. The results show that compared with the RC scheme, the ultimate bearing capacity of the two CFST schemes is increased by 115.3% and 124.2%, the initial secant stiffness is increased by 61.9% and 63.2%, and the displacement ductility coefficient is increased by 33.5% and 49.4%, respectively. The uniform circumferential confinement provided by the circular section completely eliminates the weak confinement area at the mid-span of the square steel tube wall, and the load rises steadily at the large deformation stage. The circular CFST scheme with a diameter of 560 mm, wall thickness of 16 mm, Q345 steel tube, C60 core concrete and confinement coefficient  $\xi = 0.829$  is recommended as the optimal design scheme. The research results can provide a reference for the engineering design of inclined tension rods in the cable-girder anchorage zone of low-ylon cable-stayed bridges.

## Keywords

Low-ylon cable-stayed bridge; Inclined tension rod; Concrete-filled steel tube (CFST); Confinement effect; Finite element analysis

## 1. Introduction

As a composite structural bridge type between continuous girder bridges and conventional cable-stayed bridges, low-pylon cable-stayed bridges feature low pylons and steep cables, with cable forces concentrated in limited anchorage zones, thereby exhibiting strong spanning capacity and having been widely used in railway bridge engineering. Nevertheless, as the key component transferring the concentrated forces of stay cables to the main girder, the cable-girder anchorage zone is prone to local stress concentration and concrete cracking, which constitutes a major bottleneck restricting the spanning capacity and durability of this bridge type [1-2].

To address the problems of complicated construction, large self-weight and difficult maintenance associated with traditional anchorage methods using middle webs or cross diaphragms, inclined tension rods have been adopted to replace middle webs in some newly-built railway low-pylon cable-stayed bridges. The inclined tension rods are arranged in pairs in a "herringbone" shape on the cross section of the box girder, with anchorage ends located on both sides of the box girder bottom slab and tension ends arranged at the cable-girder anchorage block in the middle of the top slab, efficiently transferring cable forces to the bottom slab and webs of the box girder[3]. However, as a new type of prestressed tensile member, the whole-process mechanical mechanism, failure mode and optimization method of traditional reinforced concrete (RC) inclined tension rods under service conditions have not been systematically studied.

Concrete-filled steel tube (CFST) can place core concrete in a triaxial compression state through the continuous confinement of the steel tube on the core concrete, significantly improving the bearing capacity and ductility of members [4-5]. Han et al.[6] revealed the composite mechanism through axial tension tests on circular CFST specimens; Zhou et al. [7] compared the axial tensile performance of circular and square CFST, pointing out that the confinement efficiency of square sections is significantly lower than that of circular sections due to the weak confinement zone at the middle of the tube wall; Xu et al. [8] established an analytical model for the strength and stiffness enhancement of circular CFST axial tension members, decomposing the improvement mechanism of core concrete on the tensile performance of steel tubes into confinement effect, fiber reinforcement effect and tension stiffening effect; Jin Kaiyuan et al. [9] conducted experimental studies on the axial tensile performance of prestressed CFST members, confirming the improvement effect of prestress level and steel ratio on tensile performance. However, all the above studies focus on single members, and research on applying prestressed CFST to the special tensile member of inclined tension rods in low-pylon cable-stayed bridges remains insufficient.

Taking the Luzhou Tuojiang Railway Super Large Bridge, a low-pylon cable-stayed bridge with a span arrangement of (146+292+146) m, as the engineering background, this paper establishes three-dimensional nonlinear finite element

models of three inclined tension rod schemes, namely RC, square CFST and circular CFST, based on ANSYS APDL parametric command flow. A systematic comparative analysis is carried out on their whole-process mechanical performance under the most unfavorable cable force, and the influence law of section forms is revealed from the perspective of confinement mechanism, providing a theoretical basis for the engineering optimization design of such members.

## **2. Engineering Background and Finite Element Model**

### **2.1. Engineering Background and Most Unfavorable Working Condition**

The main bridge of the Luzhou Tuojiang Railway Super Large Bridge adopts a single-plane prestressed concrete low-pylon cable-stayed bridge with a span arrangement of (146+292+146) m. The main girder adopts a W-shaped section with prestressed concrete inclined rods arranged longitudinally at intervals. Each pylon is equipped with 11 pairs of stay cables adopting the steel strand cable system with a standard strength of 2000 MPa.

A three-dimensional spatial frame finite element model of the whole bridge is established by using Midas/Civil. General beam elements are adopted for the main girder and pylons, while tension-only truss elements are used for stay cables. Considering comprehensive load cases including structural self-weight, secondary dead load, vertical static live load of ZKH train, and temperature load, load combinations are carried out in accordance with the Code for Design of Railway Bridges and Culverts (TB10002–2017)[10]. The maximum cable force of the whole bridge occurs at Cable M1, with a corresponding cable force of 6752.5 kN and a horizontal inclination angle of  $33.21^\circ$ . The inclined tension rod of the box girder segment where this cable is located is selected as the research object in this paper.

### **2.2. Three-Dimensional Nonlinear Finite Element Model of Inclined Tension Rod**

A three-dimensional solid finite element model of the inclined tension rod is established using the parametric command flow of ANSYS Mechanical APDL. The model adopts the unit system of N-mm-MPa, and key control parameters such as geometric dimensions, reinforcement layout and load level are centrally defined in a parametric form.

SOLID185 eight-node isoparametric solid elements are adopted for concrete, duct grouting mortar and end anchorage steel plates. Longitudinal reinforcements, stirrups and prestressing tendons are simulated by LINK180 two-node bar elements. A perfect bond assumption is adopted for the interface between steel reinforcements and concrete, and displacement compatibility is realized by node merging.

The global mesh size is set to 50 mm, and local mesh refinement up to 15 mm is applied at the circular arc of the duct. The mesh configuration and boundary

conditions of the model are illustrated in Figure 1.

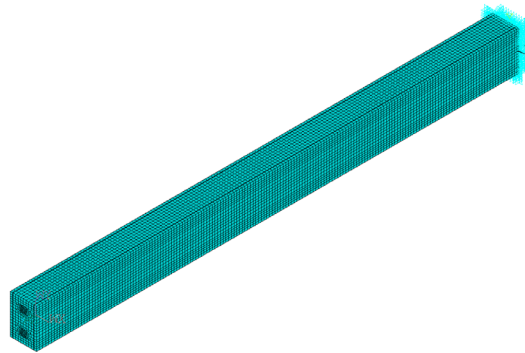


**Fig 1.** Finite-element mesh and boundary conditions of the diagonal tie rod

### 2.3. Constitutive Models and Loading Scheme

Concrete and duct grouting mortar are modeled using a modified Drucker-Prager plasticity model with tension cut-off [11]. Dilation parameters and exponential hardening/softening laws are introduced to characterize post-peak performance degradation and residual bearing capacity. The general form of the Drucker-Prager yield criterion is:

$$\sqrt{J_2} + \alpha I_1 = k$$

where  $I_1$  is the first invariant of the stress tensor,  $J_2$  is the second invariant of the deviatoric stress tensor, and  $\alpha$  and  $k$  are the friction coefficient and cohesion parameter related to the material strength parameters, respectively. Ordinary reinforcing bars, prestressing tendons, and steel tubes are all modeled using a bilinear kinematic-hardening model, while end anchorage steel plates are modeled as isotropic linear-elastic material. In the CFST schemes, in accordance with the confined-concrete constitutive theory of Mander [12], the peak strain, ultimate strain, and post-peak residual strength ratio of the core concrete are increased correspondingly with the confinement level so as to reflect the strengthening effects under the triaxial compressive state.

The confinement coefficient  $\xi$ , as a comprehensive indicator characterizing the confinement effect of the steel tube, is defined as [13]:

$$\xi = A_s \cdot f_y / A_c \cdot f_c$$

where  $A_s$  and  $A_c$  are the cross-sectional areas of the steel tube and the core concrete, respectively;  $f_y$  is the yield strength of the steel; and  $f_c$  is the axial compressive strength of the core concrete. Preliminary parametric analysis indicates that, when the confinement coefficient is in the range of 0.8-0.85, the member achieves the optimal comprehensive balance among bearing capacity, ductility, and post-peak residual bearing performance.

The loading procedure adopts a two-stage scheme of "prestressing initial equilibrium + displacement-controlled segmented loading". In the first stage, an initial tensile stress (1350 MPa) is defined within the prestressing tendons, and the model is solved to a self-equilibrium state. In the second stage, a displacement-controlled axial load is applied to the loading end and incrementally increased to the target value: the target displacement is taken as 50 mm in the CFST schemes to fully capture the response in the large-deformation stage, and 30 mm in the RC scheme. Geometric nonlinearity is activated throughout the analysis, and a force - displacement dual-criterion convergence check together with line-search activation are employed to enhance iteration robustness.

### 3. Design of Three Schemes and Comparison of Mechanical Performance

#### 3.1. Structural Design of the Three Schemes

To ensure comparability, the three schemes are kept identical in member outer-contour dimensions, length, duct positions, prestressing arrangement principle, and boundary conditions, with only the cross-sectional configuration of the diagonal tie rod differing. The detailed design parameters are listed in Table 1.

**Table 1.** Comparison of structural parameters of the three schemes

Parameter	RC scheme	Square CFST scheme	Circular CFST scheme
Cross-sectional form	Solid rectangular	Square steel tube + core concrete	Circular steel tube + core concrete
Cross-sectional dimensions / mm	400 × 600	400 × 600, t = 14	D = 560, t = 16
Longitudinal reinforcement	8 $\phi$ 22 HRB400	None	None
Stirrups	$\phi$ 12 @ 125 HRB335	None	None
Steel tube material	—	Q345	Q345
Core concrete	C60	C60	C60
Prestressing arrangement	14 strands $\phi$ s15.2 × 2 ducts	17 strands $\phi$ s15.2 × 2 ducts	17 strands $\phi$ s15.2 × 2 ducts
Confinement coefficient $\xi$	—	0.849	0.829

In the CFST schemes, the steel tube applies continuous confinement to the core concrete through interface contact from the very beginning of loading and serves simultaneously as a permanent formwork. Prestressing strands pass through two symmetrically arranged ducts within the cross-section, and an axial pre-compression reserve is imposed on the core concrete via the initial tensile stress.

#### 3.2. Comparison of Load - Displacement Curves

The full-process load - displacement curves of the three schemes are shown in Fig. 2.

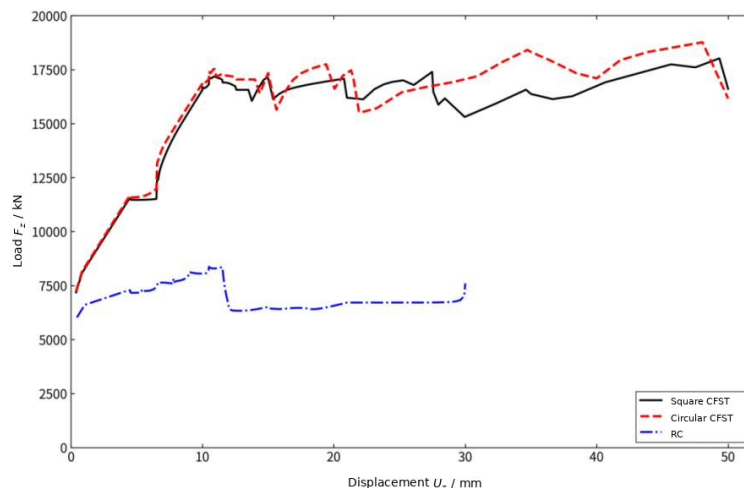


**Fig 2.** Comparison of load – displacement curves of the three schemes

As shown in Fig. 2, the load-displacement responses of all three schemes exhibit a five-stage characteristic of elastic – cracking – peak – softening – re-hardening, but the magnitudes and transition positions of each stage differ systematically owing to differences in the confinement mechanism.

In the elastic stage, the slopes of the curves of the three schemes differ markedly. The initial secant stiffness of the RC scheme is 4079 kN/mm, whereas those of the square and circular CFST schemes are 6603 kN/mm and 6656 kN/mm, corresponding to increases of 61.9 % and 63.2 % over the RC scheme, respectively. This enhancement is attributed mainly to the contribution of the steel-tube area to the equivalent axial stiffness of the cross-section and to the higher prestressing level.

In the cracking stage, macroscopic cracking in the RC scheme occurs at a displacement of 1.05 mm, corresponding to a cracking load of 6607 kN. The cracking displacements of both the square and circular CFST schemes are 0.84 mm, with cracking loads of 8075 kN and 8148 kN, respectively—increases of 22.2 % and 23.3 % over the RC scheme. The slightly smaller cracking displacements of the CFST schemes result from their higher equivalent cross-sectional stiffness, which makes the displacement required to reach the same concrete ultimate tensile strain smaller; however, the substantial increase in cracking load reveals a real enhancement of the crack-resistance reserve. Moreover, even when the core concrete cracks, the cracks are sealed inside the steel tube and do not appear on the outer surface of the member, fundamentally resolving the durability problem of exposed cracks in the RC scheme.

In the elasto-plastic ascending stage, the slope of the RC curve drops markedly after cracking and the curve enters the softening branch immediately after reaching the peak at 10.50 mm; the CFST schemes, in contrast, exhibit a sustained, approximately linear ascent until reaching the peak at around 48 mm. At a displacement of 10 mm, the loads of the square and circular CFST schemes are 2.05 and 2.09 times those of

the RC scheme at the same displacement. The mechanical mechanism of this sustained ascent lies in the fact that the continuous lateral confinement provided by the steel tube alters the path of internal-force redistribution within the cross-section: the core concrete is kept in a favorable triaxial compressive state, effectively suppressing crack penetration and damage concentration.

In terms of peak bearing capacity, the values for the RC, square CFST, and circular CFST schemes are 8373 kN, 18024 kN, and 18769 kN, respectively. The circular scheme exceeds the RC scheme by 124.2 % and the square scheme by 4.1 %. The peak displacements of the three schemes are 10.50 mm, 49.34 mm, and 48.05 mm, respectively, with the peak displacement of the CFST schemes being approximately 4.6 times that of the RC scheme. This indicates that steel-tube confinement fundamentally alters the peak-formation mechanism: the peak in the RC scheme is triggered by concrete damage localization, whereas the peak in the CFST schemes occurs only after both the steel tube and the prestressing tendons have entered a deep plastic stage.

The large-deformation stage is the key region distinguishing the two CFST schemes. The load-displacement curve of the square scheme exhibits a sustained capacity dip after a displacement of about 20 mm, with a load drop of approximately 10 %, and only re-ascends after 35 mm; in the same range, the circular scheme maintains a smooth ascent and at 30 mm the load is 12.3 % higher than that of the square scheme. The mechanical origin of the mid-segment dip in the square scheme lies in the non-uniformity of its confinement: the mid-region of the tube wall undergoes out-of-plane bending under the lateral expansion of the core concrete, causing the confinement effectiveness in this region to be markedly lower than at the corners and forming a confinement-weak band along the perimeter of the cross-section.

### 3.3. Comparison of Key Mechanical Indicators

The displacement ductility coefficient is calculated using the equal-energy bilinear method proposed by Park [14], which is insensitive to the initial-cracking point. Its basic concept is to derive an equivalent yield displacement on the principle that the area enclosed by the actual load-displacement curve is equal to that enclosed by an idealized elastic-perfectly-plastic bilinear curve; the displacement at which the post-peak capacity drops to 85 % of the peak value is taken as the ultimate displacement; and the displacement ductility coefficient is defined as the ratio of the ultimate displacement to the equivalent yield displacement. The key mechanical indicators of the three schemes are summarized in Table 2.

**Table 2.** Comparison of key mechanical performance indicators of the three schemes

Mechanical indicator	RC scheme	Square CFST	Circular CFST	Circular vs. RC
Initial secant stiffness / ( $\text{kN}\cdot\text{mm}^{-1}$ )	4079	6603	6656	+63.2 %
Cracking load / kN	6607	8075	8148	+23.3 %

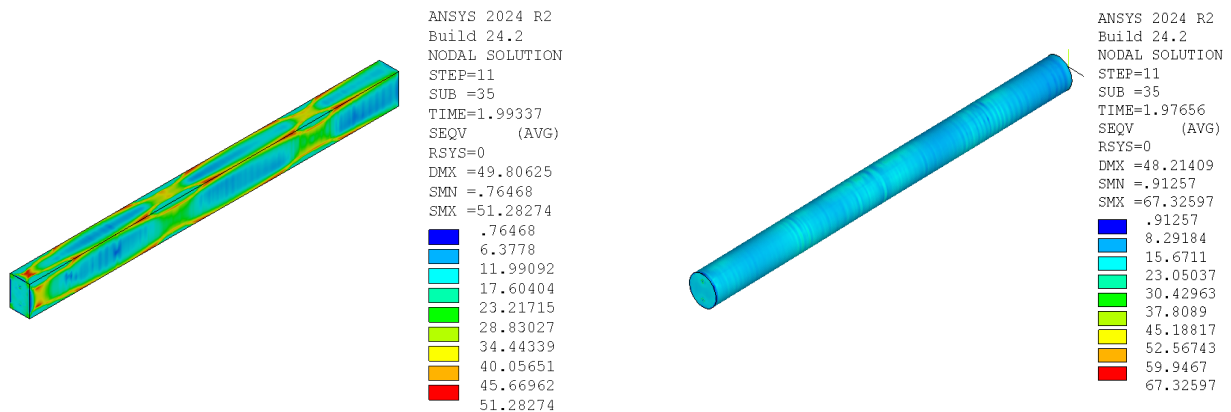
Peak bearing capacity / kN	8373	18024	18769	+124.2 %
Trough load / kN	6335	15308	15510	+144.8 %
Residual bearing ratio	0.757	0.861	0.922	+21.8 %
Equivalent yield displacement / mm	3.47	11.01	9.84	—
Ultimate displacement / mm	11.80	50.00*	50.00*	—
Displacement ductility coefficient $\mu$	3.40	4.54*	5.08*	+49.4 %

As shown in Table 2, the circular CFST scheme is superior to the square scheme on all six indicators, and both CFST schemes are far superior to the RC scheme. It should be specifically noted that, when loading of the CFST schemes is terminated at 50 mm, the bearing capacities are still maintained at 92.1 % and 86.1 % of the peak values, respectively, neither having reached the critical displacement corresponding to the post-peak 0.85  $F_{peak}$  threshold. The displacement ductility coefficients obtained by the Park equal-energy bilinear method are therefore lower-bound estimates; if loading were continued, the ductility advantages of the CFST schemes would expand further.

#### 4. Using the Template

##### 4.1. Steel Tube Stress Distribution and Confinement Mechanism

The Mises equivalent stress distributions of the two CFST schemes at the peak instant exhibit essentially different characteristics. The peak equivalent stress of the square steel tube reaches 433.4 MPa, having entered the strain-hardening stage deeply, with a yield-strength utilization ratio of 1.256. The peak equivalent stress of the circular steel tube is 397.3 MPa, with a utilization ratio of 1.152, which is 8.3 percentage points lower than that of the square tube. The differences in the confinement mechanism between the two cross-sectional shapes are illustrated in Fig. 3.



(a) Peak load moment of square CFST inclined tension rod

(b) Peak load moment of circular CFST inclined tension rod

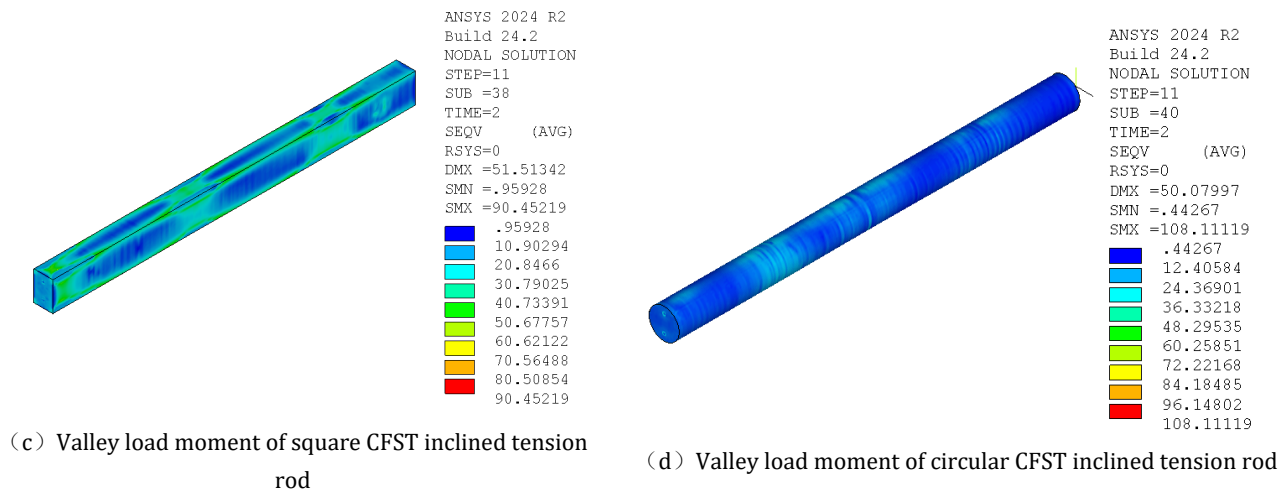


**Fig 3.** Comparison of equivalent stress distribution of the core concrete at the peak instant

The confinement stress along the perimeter of the square section is markedly non-uniform: stress concentration occurs at the four corner regions due to their higher geometric stiffness, whereas the mid-segments of the tube wall undergo out-of-plane bending under the lateral expansion of the core concrete, with relatively low local stress levels. This non-uniformity causes the corner steel tubes to yield deeply and enter the strain-hardening regime first, while the core concrete in the confinement-weak mid-segment regions undergoes damage localization and a reduction of the effective bearing area earlier, leading to a temporary drop in cross-sectional bearing capacity. With further increases in displacement, the strain-hardening of the corner concrete in the high-confinement zones gradually compensates for the capacity loss in the mid-segments, and the curve re-ascends. This "drop-then-rise" response pattern is essentially the macroscopic manifestation of the confinement non-uniformity of the square section in the load - displacement space.

Owing to the absence of geometric discontinuities, the circumferential stress in the circular section is uniformly distributed along the perimeter, all points on the tube wall approach yielding synchronously, and the core concrete is uniformly subjected to a triaxial compressive state across the entire cross-section. Damage is dispersed both circumferentially and axially, so the load - displacement curve maintains a smooth, sustained ascent during the large-deformation stage. The steel material in the circular scheme is utilized more uniformly, meaning that for the same steel input, each part of the circular cross-section contributes more uniformly to confinement and the entire cross-section can participate more fully in the confinement work, without non-uniform degradation of the confinement function caused by local premature deep hardening.

#### 4.2. Stress Safety Reserve of Prestressing Tendons and Concrete

At the peak instant, the prestressing-tendon stress in the square scheme is 2124.9

MPa (utilization ratio 1.269), whereas in the circular scheme it is 1931.7 MPa (utilization ratio 1.154). The circular scheme thus possesses a larger stress reserve in the prestressing tendons, and the safety redundancy of the prestressing anchorage system is more ample. The physical origin of this difference lies in the more severe local damage of the core concrete caused by the non-uniform confinement of the square section: the lateral expansion of the concrete in the confinement-weak mid-segment regions is partially released, the effective bearing area of the cross-section decreases, and a larger fraction of the axial load must be transferred to the prestressing tendons.

The maximum compressive stresses of the core concrete in both CFST schemes are at relatively low levels ( - 0.616 MPa and - 1.994 MPa at the peak instant, respectively), far below those of the RC scheme. This does not mean that the concrete is under-utilized; rather, it is an inevitable consequence of the reconfiguration of the force-flow path in the steel-tube - concrete composite cross-section: the steel tube places the core concrete in a triaxial compressive state through lateral confinement and bears a larger proportion of the axial load. The peak compressive stress of the core concrete in the circular scheme is 3.2 times that in the square scheme, indicating that the core concrete in the circular section participates in axial bearing to a greater extent and that the concrete material is more fully mobilized.

#### 4.3. Recommended Scheme and Structural-Level Verification

On the basis of a comprehensive comparison in terms of peak bearing capacity, large-deformation bearing stability, confinement efficiency, and safety reserve, the circular CFST scheme is comprehensively superior to the square scheme in peak bearing capacity, large-deformation bearing stability, confinement uniformity, and safety reserve, and both CFST schemes are far superior to the RC scheme. Accordingly, the circular CFST scheme (D = 560 mm, t = 16 mm, Q345 steel tube, C60 core concrete, prestressing arrangement of 17 strands  $\phi$ s15.2 in 2 ducts, confinement coefficient  $\xi = 0.829$ ) is recommended as the optimized scheme for diagonal tie rods in the cable - girder anchorage zone of extradosed cable-stayed bridges. Without changing the outer-contour dimensions of the member, this scheme achieves a synergistic enhancement of bearing capacity, ductility, and durability; in addition, the outer circular steel tube simultaneously serves as a permanent formwork, effectively simplifying the construction process.

Further structural-level verification based on an integrated three-dimensional finite-element model of the box-girder segment shows that, under the combined action of self-weight, prestressing, and ZKH train vertical live load, the circular CFST scheme increases the safety reserve coefficient of the compressive stress in the core concrete of the anchorage zone from 2.05 in the RC scheme to 3.40, an increase of 66 %. The maximum Mises equivalent stress in the outer steel tube is only 34.5 % of

its yield strength, with a safety reserve coefficient of 2.92, indicating that the steel tube remains in a deep elastic-reserve state under in-service conditions. This result confirms that the conclusions of the member-level optimization are also applicable at the structural level.

## 5. Conclusions

Taking the extradosed cable-stayed bridge of the Luzhou Tuojiang Railway Grand Bridge as the engineering background, three-dimensional nonlinear finite-element models were established for three diagonal tie rod schemes—reinforced concrete, square CFST, and circular CFST—and the mechanical performance of the three schemes under the most unfavorable cable force was comparatively analyzed. The main conclusions are summarized as follows:

(1) The failure of the RC diagonal tie rod is dominated by tensile-cracking damage localization rather than by concrete crushing. The discrete passive confinement provided by the stirrups cannot effectively suppress post-cracking damage concentration; the displacement ductility coefficient of the member is only 3.40, exhibiting a performance bottleneck that is difficult to overcome through parameter adjustment alone.

(2) Introducing prestressed concrete-filled steel tube diagonal tie rods can break through the above bottleneck at the structural-form level. The initial secant stiffness, cracking load, and peak bearing capacity of both CFST schemes increase substantially compared with the RC scheme: the circular scheme increases by 63.2 %, 23.3 %, and 124.2 %, respectively, while the square scheme increases by 61.9 %, 22.0 %, and 115.3 %; in terms of displacement ductility coefficient and residual bearing ratio, the circular scheme increases by 49.4 % and 21.8 %, respectively.

(3) The cross-sectional shape has a fundamental influence on the uniformity of the confinement mechanism. The corner-vs-mid non-uniform confinement of the square section causes the concrete in the confinement-weak mid-segment regions to undergo damage localization first, producing a marked capacity dip in the load - displacement curve during the large-deformation stage; the uniform hoop confinement provided by the circular section thoroughly eliminates the confinement-weak region, with the load increasing steadily and continuously during the large-deformation stage, and the confinement mechanism is more ideal.

(4) The circular CFST diagonal tie rod scheme ( $D = 560$  mm,  $t = 16$  mm, Q345 steel tube, C60 core concrete, confinement coefficient  $\xi = 0.829$ ) is recommended as the optimized scheme for diagonal tie rods in the cable - girder anchorage zone of extradosed cable-stayed bridges. The recommended scheme is comprehensively superior to the square scheme in bearing capacity, ductility, confinement efficiency, and safety reserve, and can serve as a reference for the design and construction of similar engineering projects.

## References

- [1] Gao C, Liu Y F, Shi D, et al. Key technologies and innovations in the design of a long-span single-cable-plane prestressed-concrete cable-stayed railway bridge: a case study of the main bridge of the Tuojiang Grand Bridge on the Longxu Railway [J]. *Railway Standard Design*, 2023, 67(12): 97–102.
- [2] Ma Y L, Chen G L. Study on the configuration selection and mechanical performance of cable-girder anchorage in prestressed-concrete extradosed cable-stayed railway bridges [J]. *Railway Standard Design*, 2022, 66(11): 88–91.
- [3] He X, Wang Z, Li C, et al. Experimental test and finite element analysis on a concrete box girder of a cable-stayed bridge with W-shaped prestressed concrete diagonal braces [J]. *Buildings*, 2024, 14(2): 506.
- [4] Cai S H, Jiao Z S. Basic behavior and strength calculation of concrete-filled steel tube short columns [J]. *Journal of Building Structures*, 1984, 5(6): 13–29.
- [5] Han L H. *Concrete-Filled Steel Tubular Structures—Theory and Practice* [M]. Beijing: Science Press, 2016.
- [6] Han L H, He S H, Liao F Y. Performance and calculations of concrete-filled steel tubes (CFST) under axial tension [J]. *Journal of Constructional Steel Research*, 2011, 67(11): 1699–1709.
- [7] Zhou M, Fan J, Tao M, et al. Experimental study on the tensile behavior of square concrete-filled steel tubes [J]. *Journal of Constructional Steel Research*, 2016, 121: 202–215.
- [8] Xu L Y, Tao M X, Zhou M. Analytical model and design formulae of circular CFSTs under axial tension [J]. *Journal of Constructional Steel Research*, 2017, 133: 214–230.
- [9] Jin K Y, Zhou X H, Wang Y H, et al. Experimental study on the axial-tension behavior of prestressed concrete-filled steel tube members [J]. *Journal of Building Structures*, 2024, 45(S1): 114–123.
- [10] National Railway Administration of China. *Code for Design on Railway Bridges and Culverts: TB 10002—2017* [S]. Beijing: China Railway Publishing House, 2017.
- [11] Guo Z H. *Strength and Constitutive Relations of Concrete: Principles and Applications* [M]. Beijing: China Architecture & Building Press, 2004.
- [12] Mander J B, Priestley M J N, Park R. Theoretical stress-strain model for confined concrete [J]. *Journal of Structural Engineering*, 1988, 114(8): 1804–1826.
- [13] Ministry of Housing and Urban-Rural Development of the People's Republic of China. *Technical Code for Concrete-Filled Steel Tubular Structures: GB 50936—2014* [S]. Beijing: China Architecture & Building Press, 2014.
- [14] Park R. Evaluation of ductility of structures and structural assemblages from laboratory testing [J]. *Bulletin of the New Zealand Society for Earthquake Engineering*, 1989, 22(3): 155–166.